Population Dynamics at High Reynolds Number

Population dynamics at high Reynolds number

Prasad Perlekar[(1)], Roberto Benzi[(2)], David R. Nelson[(3)], Federico Toschi[(1)]

[(1)] Department of Physics, and Department of Mathematics and Computer Science, and J.M. Burgerscentrum, Eindhoven University of Technology, 5600 MB Eindhoven, The Netherlands; and International Collaboration for Turbulence Research.
[(2)] Dip. di Fisica and INFN, Università "Tor Vergata", Via della Ricerca Scientifica 1, I-00133 Roma, Italy.
[(3)] Lyman Laboratory of Physics, Harvard University, Cambridge, MA 02138, USA

We study the statistical properties of population dynamics evolving in a realistic two-dimensional compressible turbulent velocity field. We show that the interplay between turbulent dynamics and population growth and saturation leads to quasi-localization and a remarkable reduction in the carrying capacity. The statistical properties of the population density are investigated and quantified via multifractal scaling analysis. We also investigate numerically the singular limit of negligibly small growth rates and delocalization of population ridges triggered by uniform advection.

PACS numbers: 47.27.-i, 47.27.E-, 87.23.Cc Keywords: Fisher equation, population dynamics, turbulence

For high nutrient concentration on a hard agar plate, the Fisher equation [1] can be a good description of the spreading of microorganisms such as bacteria at low Reynolds number [2]. However, many microorganisms, such as those in the ocean, must find ways to thrive and prosper in high Reynolds number fluid environments. In presence of a turbulent advecting velocity field $\mathbf{u}(\mathbf{x},t)$, the Fisher equation reads

$$\frac{\partial C}{\partial t} + \boldsymbol{\nabla}\cdot(\mathbf{u}C) = D\nabla^2 C + \mu C(1-C), \qquad (1)$$

where $C(\mathbf{x},t)$ is a continuous variable describing the concentration of micro-organisms, D is the diffusion coefficient and μ is the growth rate. As an example of "life at high Reynolds number", we could take Eq. (1) to represent the density of the marine cyanobacterium Synechococcus [3] under conditions of abundant nutrients, so that $\mu \sim$ constant.

As discussed in [4], an advecting compressible turbulent flow leads to highly non-trivial dynamics. Although the results of [4] were obtained only in one dimension using a synthetic advecting flow from a shell model of turbulence, two striking effects were observed: the concentration field $C(\mathbf{x},t)$ is strongly localized near transient but long-lived sinks of the turbulent flows for small enough growth rate μ; in the same limit, the space-time average concentration (denoted in the following as carrying capacity) becomes much smaller than its maximum value 1. Both effects are relevant in biological applications [5].

In this Letter, we present new numerical results for more realistic two dimensional turbulent flows. We assume that the microorganism concentration field $C(\mathbf{x},t)$, whose dynamics is described by Eq. (1), lies on a planar surface of constant height in a three dimensional fully developed turbulent flow with periodic boundary conditions. Such a system could be a rough approximation to photosynthetic microorganisms that actively control their bouyancy to manitain a fixed depth below the surface of a turbulent fluid [6]. As a consequence of this choice, the flow field in the two dimensional slice becomes compressible [7]. We consider here a turbulent advecting field $\mathbf{u}(\mathbf{x},t)$ described by the Navier-Stokes equations, and nondimensionalize time by the Kolmogorov dissipation time-scale $\tau_\eta \equiv (\nu/\epsilon)^{1/2}$ and space by the Kolmogorov length-scale $\eta \equiv (\nu^3/\epsilon)^{1/4}$, where ϵ is the mean rate of energy dissipation and ν is the kinematic viscosity. The non-dimensional numbers charecterizing the evolution of the scalar field $C(\mathbf{x},t)$ are then the Schmidt number $Sc = \nu/D$ and the non-dimensional time $\mu\tau_\eta$. A particularly interesting regime arises when the doubling time $\tau_g \equiv \mu^{-1}$ is somewhere in the middle of the inertial range of eddy turnover times ($\tau_r = r/\delta_r u$, where $\delta_r u$ is the typical velocity difference across length scale r) that characterize the turbulence. Although the underlying turbulent energy cascade is somewhat different [8], this situation arises for oceanic cyanobacteria and phytoplankton, who double in $8-12$ hours, in a medium with eddy turnover times varying from minutes to months [6].

The main results of our investigation are the following: we confirm the qualitative behaviour found in [4] for a two-dimensional population, under more realistic turbulent flow conditions. We also investigate the limit $\mu \to \infty$ and discuss the singular limit of $\mu \to 0$ validating the physical picture proposed in [4]. Our understanding of the limit $\mu\tau_\eta \ll 1$ may be helpful in future investigations, as explicit computations for $\mu > 0$ can be very demanding. In addition, we quantify the statistical properties of the concentration field and investigate the effect of an uniform convective background flow field.

We conducted a three dimensional direct numerical simulation (DNS) of homogeneous, isotropic turbulence at two different resolutions (128^3 and 512^3 collocation points) in a cubic box of length $L = 2\pi$. The Taylor mi-

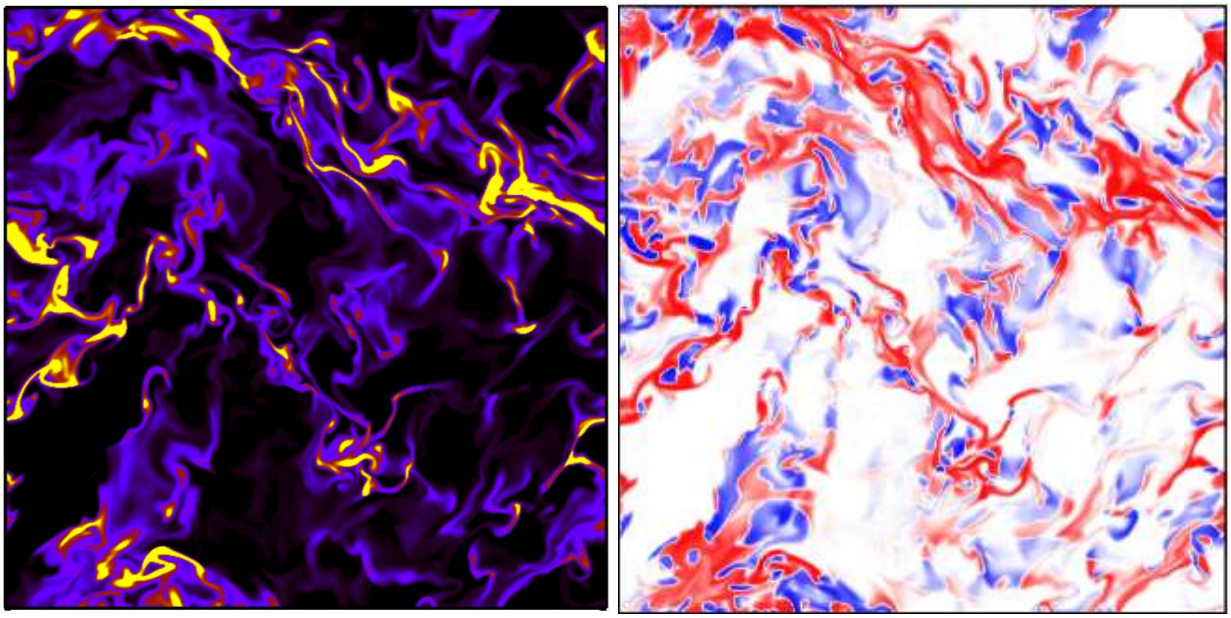

FIG. 1: (Color online) (Left panel) Pseudocolor plot of concentration field. The bright yellow regions indicate regions of high concentration ($C > 0.1$) and the black regions indicate regions of low concentration. (Right panel) Pseudocolor plot of $[C(\mathbf{x}, t_0)/(0.1 + C(\mathbf{x}, t_0))(\tanh(-\nabla \cdot \mathbf{u}))]$. The dark red regions indicate negative divergence and large concentration whereas dark blue regions indicate positive divergence and large concentration. Plot are made at identical time t_0 (after the steady state has been reached) on a slice $z = const$ obtained from our 512^2 numerical simulations of Eq. (1) for $\mu\tau_\eta = 0.0045$ and Schmidt number $Sc = 5.12$. Note that microorganisms cluster near regions of compression ($\nabla \cdot \mathbf{u} < 0$), as is evident from the high density of red regions.

croscale Reynolds number [9] for the full 3D simulation was $Re_\lambda = 75$ and 180, respectively, the dimensionless viscosities were $\nu = 0.01$ and $\nu = 2.05 \cdot 10^{-3}$, the total energy dissipation rate was around $\epsilon \simeq 1$ in both cases. For the analysis of the Fisher equation we focused only on the time evolution of a particular 2D slab taken out of the full three dimensional velocity field and evolved a concentration field $C(\mathbf{x}, t)$ constrained to lie on this plane only. This is a particularly efficient way of producing a compressible 2d velocity field in order to mimic the flow at the surface of oceans. Note that our velocity field has nothing to do with 2d turbulence and has the structures, correlations and spectra of a bidimensional cut of a fully 3d turbulent flow. A typical plot of the $2d$ concentration field and the concentration field conditioned by the corresponding velocity divergence field (taken at time $t = 86$, $Re_\lambda = 180$) in this plane is shown in Fig. 1 ($Sc = 5.12$). The Fisher equation was stepped forward using a second-order Adams-Bashforth scheme. The spatial derivatives in the diffusion operator are discretized using a central, second-order, finite-difference method. As the underlying flow field is compressible, sharp gradients in the concentration field can form during time-evolution. In order to capture these sharp fronts we use a Kurganov-Tadmor scheme for the advection of the scalar field by the velocity field [10].

The concentration $C(\mathbf{x}, t)$ is highly peaked in small areas, resembling one dimensional filaments (see Figure 1 and supplemental movie). When the microorganisms grow faster than the turnover times of a significant fraction of the turbulent eddies, $C(\mathbf{x}, t)$ grows in a quasi-static compressible velocity field and accumulates near the regions of compression, leading to filaments [15]. The geometry of the concentration field suggests that $C(\mathbf{x}, t)$ is different from zero on a set of fractal dimension d_F much smaller than 2. A box counting analysis of the fractal dimension of $C(\mathbf{x}, t)$ supports this view and provides evidence that $d_F = 1.0 \pm 0.15$.

A biologically important quantity is the spatially averaged carrying capacity or the density of biological mass in the system,

$$Z(t) = \frac{1}{L^2} \int dxdy C(\mathbf{x}; t), \tag{2}$$

and in particular its time average in the statistical steady state as a function of the growth rate μ, $\langle Z \rangle_\mu$. Without turbulence $\langle Z \rangle_\mu = 1$ for any μ. When turbulence is acting, in the limit $\mu \to \infty$ we expect the carrying capacity attains its maximum value $\langle Z \rangle_{\mu \to \infty} = 1$, because when the characteristic time τ_g becomes much smaller than the Kolmogorov dissipation time τ_η, the velocity field is a relatively small perturbation on the rapid growth of the microorganisms. Indeed, consider a perturbation expansion of $C(\mathbf{x}, t)$ in terms of τ_g. We define

$C(\mathbf{x},t) \equiv \sum_{n=0,\ldots,\infty} \tau_g^n C_n(\mathbf{x},t)$, and substitute in Eq. (1), where the functions $C_n(\mathbf{x},t)$ are the coefficients of the expansion. Upon assuming a steady state and collecting the terms up to $\mathcal{O}(\tau_g^2)$ we find, after some algebra,

$\langle Z\rangle_\mu \approx 1 - (\tau_g^2/L^2)\langle \int (\boldsymbol{\nabla}\cdot\mathbf{u})^2 \mathrm{d}\mathbf{x}\rangle + \mathcal{O}(\tau_g^3)$.

The limit $\mu \to 0$ can be investigated by noting that for $\mu = 0$, Eq. (1) reduces to the Fokker-Planck equation describing the probability distribution $\mathcal{P}(\mathbf{x},t)$ to find a Lagrangian particle subject to a time varying force field $\mathbf{u}(\mathbf{x},t)$:

$$\frac{\partial \mathcal{P}}{\partial t} + \boldsymbol{\nabla}\cdot(\mathbf{u}\mathcal{P}) = D\nabla^2\mathcal{P}. \tag{3}$$

Upon defining $\Gamma \equiv \langle(\boldsymbol{\nabla}\cdot\mathbf{u})^2\rangle^{1/2}$ as the r.m.s value of the velocity divergence, following [4] we expect a crossover in the behavior of $\langle Z\rangle_\mu$ for $\mu < \Gamma$. In the limit $\mu \to 0$, we expect:

$$\lim_{\mu\to 0}\langle Z\rangle_\mu = \frac{1}{\langle \mathcal{P}^2\rangle L^4}. \tag{4}$$

To understand Eq. (4), note first that for small μ the statistical properties of C should be close to those of $\mathcal{P}$. Thus we can assume that, in a statistical sense, $C(\mathbf{x},t) \approx L^2\langle Z\rangle_\mu \mathcal{P}(\mathbf{x},t)$. Averaging Eq. (1) in space and time leads to $\langle C\rangle_\mu - \langle C^2\rangle_\mu = 0$, which is equivalent to Eq. (4). Eq. (4) is crucial, because it allows us to predict $\langle Z\rangle_\mu$ for small μ from the knowledge of the well-studied statistical properties of Lagrangian tracer particles without growth in compressible turbulent flows. We have therefore tested both Eq. (4) and the limit $\mu \to \infty$ against our numerical simulations. In Fig. 2 we show the behavior of $\langle Z\rangle_\mu$ for the numerical simulations discussed in this Letter. The horizontal line represents the value $1/(\langle\mathcal{P}^2\rangle L^4)$ obtained by solving Eq. (3) for the same velocity field and $\mu = 0$. The insert shows a similar result for a one dimensional compressible flow [4]. For our numerical simulations we observe, for $\mu\tau_\eta > \Gamma\tau_\eta \approx 0.23$ the carrying capacity $\langle Z\rangle_\mu$ becomes close to its maximum value 1. The limit $\mu \to 0$ requires some care: the effect of turbulence is relevant for τ_g longer than the Kolmogorov dissipation time scale τ_η. We take the limit $\mu \to 0$ at *fixed* system size L. When $\tau_g \gg \tau_L \sim (L^2/\epsilon)^{1/3}$, the large scale correlation time, the population is effectively frozen on all turbulent time scales, and Eq. (4) should apply.

The limit $\mu \to 0$ can be investigated more precisely as follows: according to known results on Lagrangian particles in compressible turbulent flows, $\mathcal{P}$ should have a multifractal structure in the inviscid limit $\nu \to 0$ [7, 11, 12]. If our assumption leading to Eq. (4) is correct, $C(\mathbf{x},t)$ must show multifractal behavior in the same limit with multifractal exponents similar to those of $\mathcal{P}$.

We perform a multifractal analysis of the concentration field $C(x,y,t)$ with $\mu > 0$ by considering the average quantity $\tilde{C}_\mu(r,t) \equiv \frac{1}{r^2}\int_{B(r)} C(x,y,t)dxdy$ where $B(r)$ is a square box of size r. Then the quantities $\langle \tilde{C}_\mu(r)^p\rangle$ are expected to be scaling functions of r, i.e. $\langle \tilde{C}_\mu(r)^p\rangle \sim r^{a(p)}$, where $a(p)$ is a non linear function of p.

In Figure 2 we show the quantity $a(p)$ for $\mu = 0, 0.1$, and 1 for $0 \le p \le 4$ extracted from power law fits to $\langle \tilde{C}(r)^p\rangle$ over ~ 1.5 decades. In the inset we show $\langle \tilde{C}(r)^2\rangle$ for $\mu = 0.01$. Although our dynamic range is limited, the scaling description seems to work with smoothly varying exponents $a(p)$. Even more important, the statistical properties of $\tilde{C}_\mu(r)$ seems to converge to the case $\mu = 0$ as $\mu \to 0$. In the same figure we also show, for comparison, a similar analysis performed for the energy dissipation field (black line); see [9] for a detailed description.

Our multifractal analysis suggests a relation between the quasi localization length ξ and the carrying capacity $\langle Z\rangle_\mu$. The quasi localization length ξ can be considered as the smallest scale below which one should not observe fluctuations of $C(\mathbf{x},t)$. In the limit $\mu \to 0$, we can define the quasi localization length ξ as:

$$\xi^2 \equiv \frac{\langle \mathcal{P}^2\rangle}{\langle(\nabla\mathcal{P})^2\rangle}. \tag{5}$$

We expect ξ to be of the same order of the width of the narrow filaments in Fig. 1. To compute $\langle Z\rangle_\mu$ as a function of ξ, we observe that it is reasonable to assume $\langle \mathcal{P}^2(\mathbf{x},t)\rangle \sim \langle C^2(r=\xi,t)\rangle \sim \xi^{a(2)}$. Using Eq. (4) we obtain $\langle Z\rangle_\mu \sim \xi^{-a(2)}$. On the left side of Figure 3 we show $\langle Z\rangle_\mu$ as a function of ξ (obtained by using (5)) for $\mu = 0.01$ by varying the diffusivitiy D. Reducing the diffusivity D shrinks the localization length ξ and $\langle Z\rangle_\mu$ becomes smaller. Dimensional analysis applied to Eq. 3 and 5 suggests that $\xi \propto (D^2\nu/\epsilon)^{1/4}$. More generally we expect that $\xi(D)$ is monotonically increasing with D. From Figure 3 (left side), a reasonable power law behavior is observed with a scaling exponent 0.46 ± 0.03 very close to the predicted behavior $-a(2) = 0.47$ obtained from Fig. 2 (right side inset).

Note that Fig. 3 (left side) reveals a strong dependence of $\langle Z\rangle_\mu$ on ξ and hence on the microbial diffusion constant. D in turn depends on the ability of marine microorganisms to swim. Approximately 1/3 of the open ocean isolates of *S*ynechococcus can propel themselves along their micron-sized long axis at velocities of $\sim 25\mu m/sec$ [13]. Upon assuming a random direction change every $\sim 20-30$ body lengths, the effective diffusion constant entering Eq. (1) can be enhanced $1000-$fold relative to D for passive organisms. The extensive energy investment required for swimming in a turbulent ocean becomes more understandable in light of the increased carrying capacity associated with say, a $\sim 30-$fold increase in ξ. Some marine microorganisms may have evolved swimming in order to mitigate the overcrowding associated with compressible turbulent advection.

Finally, we discuss bacterial populations subject to both turbulence and uniform drift because of, e.g., the ability to swim in a particular direction. In this case, we

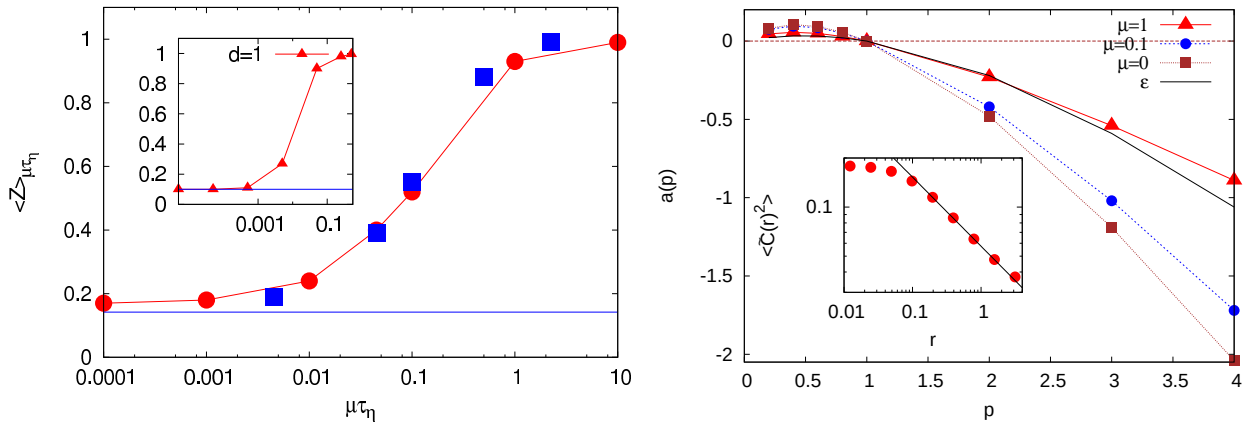

FIG. 2: (Color online) Left panel: Behavior of the carrying capacity $\langle Z\rangle_{\mu\tau_\eta}$ as a function of $\mu\tau_\eta$ from 128^2 (red dots) and 512^2 (blue squares) numerical simulations with $Sc = 1$. Note that for $\mu\tau_\eta \lesssim 0.001$, the carrying capacity approaches the limit $1/(\langle \mathcal{P}^2\rangle L^4) \approx 0.16 \pm 0.02$ (blue line) predicted by Eq. (4). In the inset we show similar results for one dimensional compressible turbulent flows in [4]. Right panel: The anomalous exponents $a(p)$ computed by the multifractal analysis of the concentration field $C(\mathbf{x}, t)$ for different values of μ and $Sc = 1$ for our 512^2 numerical simulation. Note that for $\mu \to 0$ the multifractal exponents approach the statistical properties of the field $\mathcal{P}$ described by Eq. (3). The black line shows the multifractal properties of the energy dissipation rate ϵ. In the inset we show the scaling behavior of $\langle \tilde{C}(r)^2\rangle$ for $\mu = 0.1$.

can decompose the velocity field into zero mean turbulence fluctuations plus a constant drift velocity u_0 [14] along e.g. the x-direction. In presence of a mean drift velocity Eq. (1) becomes:

$$\frac{\partial C}{\partial t} + \boldsymbol{\nabla} \cdot [(\mathbf{u} + u_0 \hat{\boldsymbol{e}_x})C] = D\nabla^2 C + \mu C(1 - C) \qquad (6)$$

where $\hat{\boldsymbol{e}_x}$ is the unit vector along the x-direction. Note that a mean drift (to follow nutrient gradients, say) breaks the Galilean invariance as the concentration C is advected by u_0, while turbulent fluctuations $\mathbf{u}$ remain fixed. In Fig. 3 we show the variation of carrying capacity versus u_0 for two different values of μ and fixed diffusivity $D = 0.015$. We find that for $u_0 \lesssim u_{rms}$ (the root-mean-square turbulent velocity) the carrying capacity Z saturates to a value equal to the value of Z in absence of u_0 i.e., quasilocalization by compressible turbulence dominates the dynamics. For $u_0 > u_{rms}$ the drift velocity delocalizes the bacterial density eventually causing $Z \to 1$, as was also found in $d = 1$.

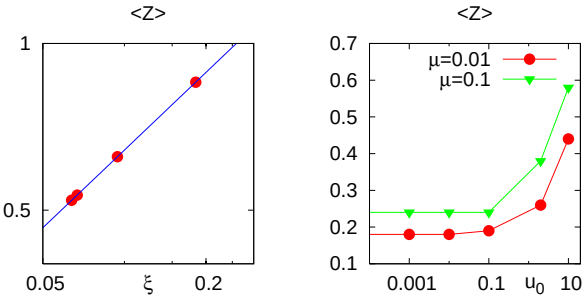

FIG. 3: (Color online) Left: Log-log plot of $\langle Z\rangle$ as a function of the localization length ξ defined in Eq. (5) for $u_0 = 0$. The blue line is the fit to the power-law. The slope is consistent with the prediction $\langle Z\rangle \sim \xi^{-a(2)}$ discussed in the text. The numerical simulations are done for $\mu = 0.01$ and different values of D from $D = 0.05$ to $D = 0.001$. Right: Plot of $\langle Z\rangle$ as function of a super-imposed uniform velocity u_0 for $\mu = 0.01$ (red bullets) and $\mu = 0.1$ (green triangles) with $D = 0.015$.

Acknowledgment We thank M.H. Jensen, A. Mahadevan, S. Pigolotti, and A. Samuel for useful discussions. We acknowledge computational support from CASPUR (Roma, Italy uner HPC Grant 2009 N. 310), from CINECA (Bologna, Italy) and SARA (Amsterdam, The Netherlands). Support for D.R.N. was provided in part by the National Science Foundation through Grant DMR-0654191 and by the Harvard Materials Research Science and Engineering Center through NSF Grant

DMR-0820484. Data from this study are publicly available in unprocessed raw format from the iCFDdatabase (http://mp0806.cineca.it/icfd.php).

[1] R.A. Fisher, *Ann. Eugenics*, **7**, 335 (1937); A. Kolmogorov, I. Petrovsky, and N. Psicounoff, Moscow, *Univ. Bull. Math.*, **1**, 1 (1937).
[2] J. Wakita et al., *J. Phys. Soc. Jpn.*, **63**, 1205 (1994).
[3] L.R. Moore, R. Goerrcke, and S.W. Chisholm, *Mar. Ecol. Prog. Ser.*, **116**, 259 (1995).
[4] R. Benzi and D.R. Nelson, *P*hysica D, *238*, 2003 (2009).
[5] J.D. Murray, *Mathematical Biology* (Springer, Berlin, 1993); D.R. Nelson and N.M. Shnerb, *Phys. Rev. E*, **58**, 1383 (1998).
[6] A.P. Martin, *Prog. in Oceanography*, **57**, 125 (2003).
[7] G. Boffetta, J. Davoudi, B. Eckhardt, and J. Schumacher, *Phys. Rev. Lett.*, **93**, 134501 (2004).
[8] W.J. McKiver and Z. Neufeld, *Phys. Rev. E*, **79**, 061902 (2009).
[9] U. Frisch, *Turbulence the legacy of A.N. Kolmogorov* (Cambridge University Press, Cambridge, 1996).
[10] A. Kurganov and E. Tadmor, *J. Comp. Phys.*, **160**, 241 (2000).
[11] J. Bec, *Phys. Fluids*, **15**, L81 (2003); J. Bec, J. Fluid Mech., **528**, 914 (2001).
[12] G. Falkovich, K. Gawedzki, and M. Vergassola, *Rev. Mod. Phys.*, **73**, 914 (2001).
[13] K. M. Ehlers et al., *Proc. Natl. Acad. Sci.*, **93**, 8340 (1996), see also E. M. Purcell, *Am. J. Phys.*, **45**, 3 (1977).
[14] A.V. Straube and A. Pikovsky, *Phys. Rev. Lett.*, **99** 184503 (2007).
[15] In two-dimensions, locally, the flow can be characterized by determinant and the divergence of the velocity gradient tensor $\nabla\mathbf{u}$. Negative (positive) values of $\nabla \cdot \mathbf{u}$ correspond to regions of compression (expansion) whereas negative (positive) values of the $det(\nabla\mathbf{u})$ correspond to regions of strain (vorticity).